Electronic structure of $FeSi_{1-x}Ge_x$ and $FeGa_3$ investigated by soft x-ray photoelectron spectroscopy complementary to x-ray emission spectroscopy

H. Yamaoka,[1] M. Matsunami,[1,2] R. Eguchi,[1,2] Y. Ishida,[1] N. Tsujii,[3] Y. Takahashi,[4] Y. Senba,[5] H. Ohashi,[5] and S. Shin[1,2]

[1]*Harima Institute, RIKEN (The Institute of Physical and Chemical Research), Sayo, Hyogo 679-5148, Japan*

[2]*Institute of Solid State Physics, University of Tokyo, Kashiwa, Chiba 277-85817, Japan*

[3]*Quantum Beam Center, National Institute for Materials Science, 1-2-1 Sengen, Tsukuba 305-0047, Japan*

[4]*University of Hyogo, 3-2-1 Kouto, Kamigori, Ako, Hyogo 678-1297, Japan*

[5]*Japan Synchrotron Research Institute, Sayo, Hyogo 679-5148, Japan*

(Received 10 April 2008; revised manuscript received 24 June 2008; published 30 July 2008)

Soft x-ray photoelectron spectroscopy for $FeSi_{1-x}Ge_x$ ($x=0$, 0.11, 0.19, 0.26, and 0.44) and $FeGa_3$ was performed at Fe L absorption edge complementary to the x-ray emission spectroscopy. The absorption and valence-band spectra show the phase transition of the electronic state between $x=0.26$ and 0.44 in $FeSi_{1-x}Ge_x$ accompanying the narrowing of the density of state near the Fermi edge. High-resolution x-ray absorption spectra (total electron yields) at Fe $2p_{3/2}$ absorption edge resolve the fine structure, originated from the valence and Auger component of electrons. Resonant valence-band and constant initial-state spectra show Fano-type profile at Fe $2p_{3/2}$ absorption edge only for the $x=0.44$ sample but not for the $x=0$ sample and $FeGa_3$. The crossover point, where the Raman and Auger features mix, is near the Fe $2p$ absorption edge for both of the $x=0$ and 0.44 samples, showing the delocalized $3d$ states.

DOI: 10.1103/PhysRevB.78.045125 PACS number(s): 71.20.Be, 71.30.+h, 79.60.−i

I. INTRODUCTION

Semiconducting behaviors with the gap in $3d$ energy bands have been observed in Fe-based intermetallic compounds, such as FeSi,[1] $FeGa_3$,[2] Fe_2VAl,[3] $FeSb_2$,[4] and $FeSi_2$.[5] Among them, unusual magnetic and transport properties of FeSi have drawn great interest for many decades after the investigation by Jaccarino *et al.*[1] FeSi has $B20$ structure with the cubic space group $P2_13$, lacking a center of symmetry. The formation of the narrow gap of ~60 meV at low temperature was confirmed by high-resolution laser photoelectron spectroscopy (PES).[6] The magnetic susceptibility increases drastically above 100 K, reaching a maximum near 540 K. This behavior at high temperatures can be described by a Curie-Weiss law, indicating presence of magnetic moment.

Theoretical models for FeSi have been proposed. These models include local-density approximation (LDA),[7] extended LDA+U method,[8] two-band Hubbard model,[9,10] LDA calculations for supercells by taking into account of thermally induced lattice disorder,[11] first-principles all-electron-density-functional calculations,[12] and spin-fluctuation theory.[13] Aeppli and Fisk[14] proposed the Kondo insulator (KI) model by considering its similarity to f valence fluctuation system: the gap-closure temperature being too low to result from a simple thermal activation mechanism. The LDA band theory, however, indicated that FeSi has a broad Fe $3d$-Si $3p$ band and both Si and Fe have neutral valences.[8,15] Thus the results of band calculations are inconsistent with the intermediate-valence KI picture.

On the other hand, the isoelectronic compound FeGe is a long-range spiral metallic ferromagnet with a transition to helimagnetic order at 280 K and it has the same crystal structure as FeSi.[16] This helical order is suppressed at 19 GPa.[17] Recent optical study for FeGe shows the evidence of heavy charge carrier.[18]

Therefore Ge substitution of the Si sites of FeSi offers another candidate to study the semiconducting to ferromagnet metal transition.[19–26] Experimentally Yeo *et al.*[25] found that Ge substitution to Si sites of FeSi induces a semiconductor to ferromagnetic metal transition around $x=0.25$ for $FeSi_{1-x}Ge_x$, where x is Ge concentration. Anisimov *et al.*[24] carried out LDA+U calculations on $FeSi_{1-x}Ge_x$ and predicted a first-order insulator to metal transition (IMT) at around $x=0.4$. Recent spin-polarized band calculations show that the small band gap closes for $x \geq 0.3$ due to the substitutional disorder and volume expansion.[26] The insulator phase $FeSi_{1-x}Ge_x$ has a small gap and in the magnetic phase the density of states (DOS) around Fermi level changes. Thus the electronic structure is apparently important to understand the characteristics of $FeSi_{1-x}Ge_x$. Spectroscopic methods such as x-ray emission spectroscopy (XES) and PES are suited for probing the electronic structure of these materials directly.[27]

Recently we performed the XES including the measurements of partial fluorescence yield and resonant inelastic x-ray scattering for $FeSi_{1-x}Ge_x$.[28] The $K\beta$ x-ray emission data provide evidence of the transition from low spin (LS) to high spin (HS) with increasing x. We note that, although the x-ray spectroscopic data suggest a prolonged transition of the spin state, XES yields information about the averaged local on-site magnetic moments. Thus, while apparently progressive at a macroscopic scale, this transition possibly corresponds to a superposition of nonmagnetic and magnetic Fe states, the ratio of the latter increasing monotonously with Ge doping. The valence spectra of the PES are expected to show the change due to the long-range magnetic order or IMT. Delocalization and high degree of covalence for the Fe $3d$ states in FeSi are also deduced from the $1s3p$ resonant XES. Our XES results support the LDA band theory but are inconsistent with KI picture that assumes the intermediate-valence admixture.

In this paper we report the experimental results of the soft x-ray photoelectron spectroscopy for $FeSi_{1-x}Ge_x$ and $FeGa_3$. $FeGa_3$ was measured for comparison as a reference sample of the narrow gap semiconductor and also known having a potential of thermoelectric materials.[29] The PES has not been applied to Ge-doped system of $FeSi_{1-x}Ge_x$ so far. We employed the PES to obtain complementary information to the XES mentioned above.[28,27] One of the purposes in this study is to confirm the IMT from the viewpoint of the electronic structure because in the $K\beta$ XES the intensity of the up spin seemed to increase monotonously with Ge doping. The valence-band spectra of the PES in this study show that the electronic state changes between $x=0.26$ and 0.44 of $FeSi_{1-x}Ge_x$, where the IMT occurs. Resonant photoelectron spectroscopy is performed for the $x=0$ and 0.44 samples at Fe $2p_{3/2}$ absorption edge. We found in constant initial state (CIS) that Fano-type profile is observed around the point, where the Raman and Auger features crossover, only for $x=0.44$ sample.

II. EXPERIMENT

Polycrystalline samples of $FeSi_{1-x}Ge_x$ and $FeGa_3$ were prepared by argon arc melting from pure metals and annealing in evacuated silica tubes. The Si/Ge composition in $FeSi_{1-x}Ge_x$ was determined by the energy dispersive x-ray spectroscopy. Powder x-ray diffraction confirmed that all the samples ($x=0$, 0.11, 0.19, 0.26, and 0.44) of $FeSi_{1-x}Ge_x$ were in single phase with the cubic $B20$ structure. Magnetic susceptibilities of $x=0$, 0.11, 0.19, and 0.26 show gaplike behavior, while that of $x=0.44$ shows ferromagnetic transition at low temperature.[28,30] This is in agreement with the previous results of Yeo *et al.*[25] The transition occurs between $x=0.2$ and 0.44. $FeGa_3$ was measured as a reference sample, which has a larger gap compared to $FeSi$[2].[29,31,32] Single crystals were grown by a Ga-flux method as described earlier.[31] Powder x-ray diffraction confirmed the $FeGa_3$-type crystal structure, with space group $P42/mnm$.

Soft x-ray PES was performed at the BL17SU undulator beamline in SPring-8 (Ref. 33) with a hemispherical electron analyzer SCIENTA SES 2002.[31,34] The resolution ΔE was estimated to be about 0.4 eV from Au valence spectra, where E is emitted electron energy. The measurements were performed on clean surfaces by fracturing the samples at 53–55 K under the vacuum pressure below $(2-3)\times10^{-8}$ Pa. Au $4f$ lines were used to correct the measured photoelectron energy in every measurement when the incident photon energy was changed.

III. RESULTS AND DISCUSSION

Figure 1(a) shows x-ray absorption spectroscopy (XAS) spectra (total electron yields) of the $x=0$, 0.11, 0.19, 0.26, and 0.44 samples of $FeSi_{1-x}Ge_x$ and $FeGa_3$ samples as a function of the incident photon energies. The intensities are normalized to the peaks. High-resolution XAS at Fe $2p_{3/2}$ absorption edge resolves the fine structure, originated from the valence and Auger component of electrons, as will be described later. We can clearly see large change in the shape

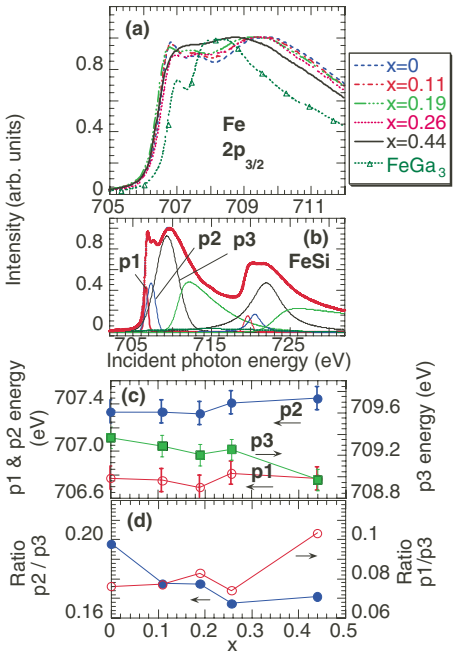

FIG. 1. (Color online) (a) The absorption spectra (total electron yields) as a function of the incident photon energies at Fe $2p_{3/2}$ absorption edge for $x=0$, 0.11, 0.19, 0.26, and 0.44 and for $FeGa_3$. (b) Example of the curve fitting. (c) Peak energies of $p1$, $p2$, and $p3$ as a function of the incident photon energies. (d) Intensities of $p1$ and $p2$ normalized by that of $p3$ as a function of x.

of the spectra at $x=0.44$. No chemical shift due to the change in the Fe charge state of $FeSi_{1-x}Ge_x$ is observed at the Fe $2p_{3/2}$ absorption edge. This indicates that the Ge doping does not affect the neutral Fe valence.[28] The absorption spectrum of $FeGa_3$, however, shows the differences from those of $FeSi_{1-x}Ge_x$: a small shift of the absorption edge to higher energy, decrease in pre-edge peak intensity at 707 eV, and large shift of the white peak to lower energy. An example of the curve fitting for the XAS of FeSi ($x=0$) is shown in Fig. 1(b). We simply assumed three components of $p1$, $p2$, and $p3$ for $2p_{3/2}$ and $2p_{1/2}$ as well. The peak energy and intensity ratio as a function of x are estimated as shown in Figs. 1(c) and 1(d). The peak energy of $p3$ shows a large shift at $x=0.44$, but those of $p1$ and $p2$ do little. The intensity ratio of $p1$ to $p3$ shows large change between $x=0.26$ and 0.44, while that of $p2$ to $p3$ gradually decreases. The increase in the ratio $p1/p3$ for $x=0.44$ is due to the decrease in the $p3$ intensity, while $p2/p3$ remains almost unchanged. As will be shown later, the peaks of $p1$ and $p3$ originate from the $3d$ valence (mainly $F1$ and $F2$) and Auger electrons, respectively. Peak $p2$ has both contributions. The results in Fig. 1 indicate clearly that the electronic state makes the transition between $x=0.26$ and 0.44 samples of $FeSi_{1-x}Ge_x$.

Figure 2(a) shows valence-band spectra of $x=0$, 0.11, 0.19, 0.26, and 0.44 of $FeSi_{1-x}Ge_x$ and $FeGa_3$ at the incident photon energy of 1102 eV at 53–55 K. Expanded view of Fig. 2(a) around Fermi edge is shown in Fig. 2(b). The intensities are normalized by the areas. The peaks at the binding energies of 0.2 and 2 eV are denoted as $F1$ and $F2$ in $FeSi_{1-x}Ge_x$, respectively. In $FeSi_{1-x}Ge_x$ these peaks show clear change in increasing Ge doping from $x=0.26$ to 0.44 as

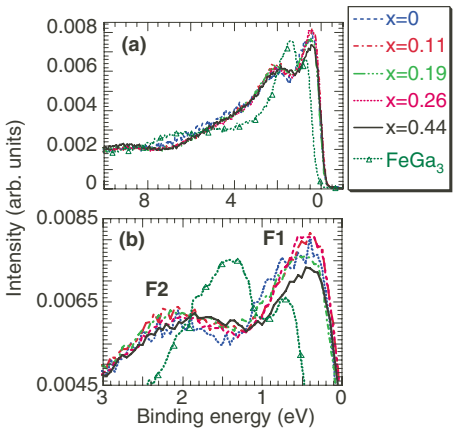

FIG. 2. (Color online) The valence spectra of $FeSi_{1-x}Ge_x$ at the incident photon energy of 1102 eV at 53–55 K. (a) Valence-band spectra as a function of x of $FeSi_{1-x}Ge_x$ and $FeGa_3$. (b) Expanded view of the valence spectra around Fermi edge.

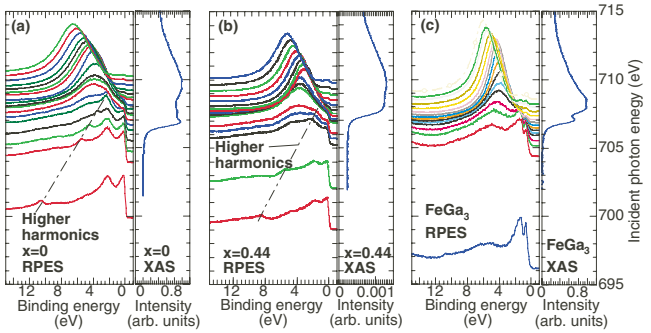

FIG. 3. (Color online) Resonant valence-band spectra at Fe $2p_{3/2}$ absorption edge at (a) $x=0$ (FeSi), (b) $x=0.44$ of $FeSi_{1-x}Ge_x$, and (c) $FeGa_3$ with the absorption spectra. The vertical position of the resonant valence-band spectra in the left panel with regard to the absorption spectrum in the right panel corresponds to the incident energy they were collected at.

well as in the XAS spectra. The valence-band spectrum of $FeGa_3$ shows larger energy gap more than 0.4 eV compared to $FeSi_{1-x}Ge_x$.[31] The valence-band spectrum of $FeGa_3$ has similar structure to those of $FeSi_{1-x}Ge_x$. The structure is explained by the band calculations: the sharp peak at 0.5 eV and the broad distribution around 0.5–3 eV below the Fermi edge correspond to nonbonding Fe $3d$ states and hybridized Fe $3d$-Ga $4p$ states,[2,32] respectively. In Fig. 2(b) the energy of $F2$ peak in $FeSi_{1-x}Ge_x$ shifts toward the Fermi edge, while the relative intensity of the $F1$ decreases. This indicates the narrowing of the DOS near the Fermi edge.

The structure of our valence-band spectra of $FeSi_{1-x}Ge_x$ agrees with results of band calculations. Anisimov *et al.*,[8] for instance, showed in LDA+U calculation of FeSi that two peaks appear in DOS around 1 and 2 eV below the Fermi energy. Fu *et al.*[35] showed that bands close to the Fermi energy have predominant $3d$ character and their hybridization with Si s-p states is very small. These results enable us to conclude that spectral peaks $F1$ and $F2$ in Fig. 2(b) correspond to the nonbonding Fe $3d$ states and slightly hybridized $3d$ states with Si s-p orbitals, respectively, bearing a close resemblance to the valence-band spectra of $FeGa_3$.[2,32]

Change in the valence spectra in $FeSi_{1-x}Ge_x$ is also consistent with the results of band-structure calculations in agreement with XES measurements: the Ge doping causes the volume to increase that leads to the narrowing of the Fe $3d$ bandwidth, although its effect is relatively weak compared to other dopants.[11,26] From the comparison of the calculated DOSs of FeSi and FeGe, Anisimov *et al.*[24] indicated that the unusual IMT from insulating to metallic ferromagnetic state is driven by the narrowing, rather than increasing, the bandwidth. The band calculation for supercell by Jarlborg[26] indicated that as the result of disorder introduced by the Ge doping, the energy gap is reduced. On the other hand, Bharathi *et al.*[20] calculated the DOS for FeSi and FeGe in a wide energy range. They also showed the narrowing of the DOS for FeGe. The following is our scenario of an explanation. On the occurrence of the exchange splitting with conserving the total electron number, the DOS of the minority-spin electrons just below the Fermi level partly shifts upward above the Fermi level, while that of the majority electrons shifts downward. This leads to the relative increase and decrease in $F2$ and $F1$ peak intensities, respectively. The gaplike structure will still remain even in the metallic phase. Observed spectral change therefore results from the superposition of the band narrowing due to local volume expansion and the occurrence of the exchange splitting. We should, however, be careful to draw some definite conclusions because of the lack of enough resolution of our present measurements. Thus we simply conclude the narrowing of the DOS near the Fermi edge after the phase transition, accompanying the relative decrease in nonbonded $F1$ DOS, i.e., slightly hybridized states of Fe $3d$, and thus causing the Stoner-type DOS splitting.

We note that Fu *et al.*[35] denied the KI picture for FeSi, where the narrow band hybridized with conduction band, and concluded that FeSi is strongly correlated insulator. Anisimov *et al.*[8,24] regarded FeSi as neutral Fe in crystal Si, in disagreement with the KI picture. These conclusions are supported also by our experimental results of the PES: the absorption edges of the total electron yields do not change by the Ge doping and the valence-band spectra are well explained by the band calculations. Similar structure of the valence spectrum on $FeGa_3$ may support its same band picture as the FeSi case.

Meanwhile, the measurements of the XES showed that the HS state increased monotonously with the Ge doping.[28] Two explanations will be possible. The lattice constant of $FeSi_{1-x}Ge_x$ previously exhibits a monotonous increase with x up to 0.25 without structural phase transition.[20] The Ge substitution of Si sites in FeSi produces a negative local chemical pressure, i.e., a local lattice expansion around Ge ions. The induced enhancement of the local density of states on the nearest-neighbor Fe sites favors the appearance of magnetic moments. The increase in the $K_{\beta'}$ intensity with Ge concentration therefore signifies the appearance of local magnetic moments on Fe sites. One may interpret this transition as a superposition of LS and HS states, with the latter component increasing upon the doping-induced local lattice expansions. Another possibility will be attributed to the lack of the data point. Although this study does not include spec-

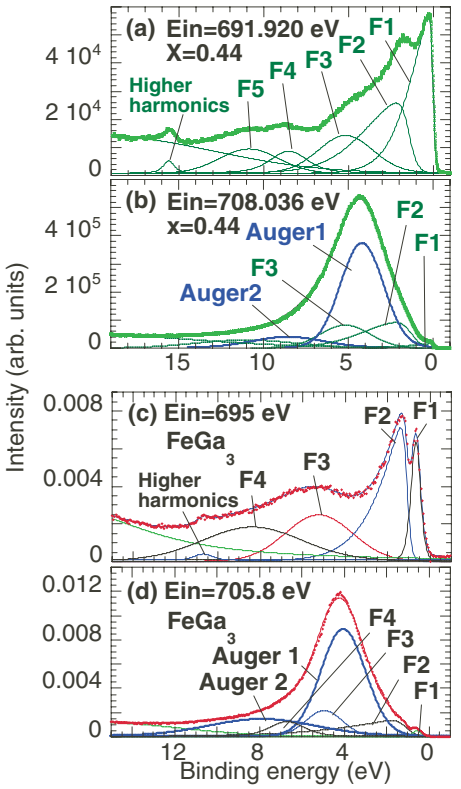

FIG. 4. (Color online) Examples of the curve fitting for the $x=0.44$ sample of $FeSi_{1-x}Ge_x$ at the incident photon energies of (a) $E_{in}=691.920$ and (b) 708.036 eV and for $FeGa_3$ at (c) $E_{in}=695.0$ and (d) 705.8 eV.

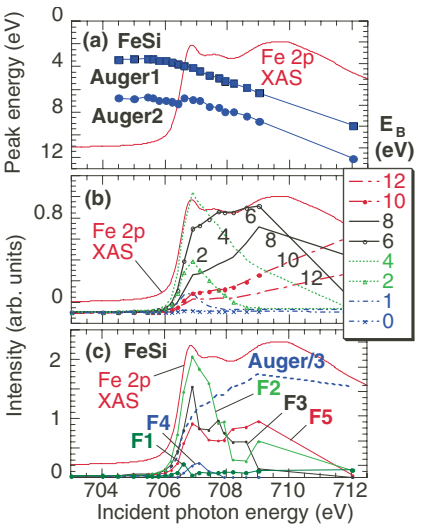

FIG. 5. (Color online) Results of analyses for $x=0$ as a function of the incident photon energies with the Fe $2p_{3/2}$ absorption spectra. (a) Peak energies of the Auger lines. (b) Change in the intensity of the constant initial states at given binding energies (E_B). The labeled numbers in the figure correspond to the binding energies. (c) Results of the curve fit in Fig. 4: change in the $F1-F5$ intensities with Auger intensity. Two Auger line intensities are summed and one-third intensity is shown.

tra in the corresponding doping range, one may anticipate the magnetic moment to increase discontinuously when entering the ferromagnetic phase at $x=0.25$.

We note that the XES provides information about the averaged local on-site magnetic moments. To the contrary, the valence-band spectra are sensitive to the change in the DOS and the Fermi level, as a result of the long-range magnetic order. Thus we can observe the change in the valence-band spectra between $x=0.26$ and 0.44, where the IMT is expected.

The measurements of the resonant valence-band spectra as a function of the incident photon energies are performed as shown in Fig. 3, (a) $x=0$ and (b) $x=0.44$ of $FeSi_{1-x}Ge_x$ and (c) $FeGa_3$ with the XAS spectra. The intensities are normalized by the areas. A small peak due to higher harmonics of the incident photon beam can be seen. We observe the photoemission–like or resonant Raman valence-band spectra below the absorption edge, where the binding energy does not depend on the incident photon energies. This is one-step or coherent process, whereas, the Auger-type behavior is observed above the absorption edge, corresponding to two-step or incoherent process. The Auger spectra show incident energy dependence. These processes are described by the Kramers-Heisenberg formula.[36] They compete with each other around the absorption edge, depending on the time of core-hole decay and screening due to charge transfer.[37] In the $3d$ transition metals and metal compounds, the relaxation due to the charge transfer or screening is likely to occur so quickly that the two-step Auger process becomes more dominant over the Raman process. Therefore, if the Raman region is restricted below the absorption edge, the relaxation process is dominant and the $3d$ electrons are relatively delocalized. While, if the $3d$ electrons are well localized before the relaxation of the core hole, the extra photon energy is transferred to the outgoing electrons. For example, in NiO and CuO, the relaxation time may be comparable to core-hole lifetime. The Raman feature was observed over the energy of absorption edges and the $3d$ electron states are kept to be localized.[38,39] If the both regimes coexist, the interference effect could be expected. We add the fact that in Ni or V metals the valence spectra showed two-hole satellite.[40–42] This effect has been explained by the Kotani-Toyozawa model[40] that takes into account of the two-step screening.

We made the curve fitting to separate the Auger and Raman contributions to the valence spectra in Fig. 3, assuming several symmetric and asymmetric profiles for simplicity. Examples of the curve fitting for the valence-band spectra are shown in Figs. 4(a) and 4(b) for $x=0.44$ sample of $FeSi_{1-x}Ge_x$ at the incident photon energies $E_{in}=691.920$ and 708.036, respectively, and Figs. 4(c) and 4(d) for $FeGa_3$ at $E_{in}=695.0$ and 705.8. For $FeGa_3$ we used similar notations as those for $FeSi_{1-x}Ge_x$. We separate the Auger peak into two parts due to the asymmetry of the profile. The LDA band calculations for FeSi show that the peaks around 1, 3, 6, and 9 eV in the valence band, respectively, correspond to the states of Fe $3d$, Fe $3d$, Si $3p$, and Si $3s$.[7,8] In our valence-band spectra of $FeSi_{1-x}Ge_x$ they correspond to $F1$ (0.5 eV), $F2$ (2 eV), $F3$ (5 eV), and $F4$ (8 eV), considering the energy shift due to the background.[43]

The results of analysis for resonant PES as a function of the incident photon energies are shown in Fig. 5 ($x=0$), Fig.

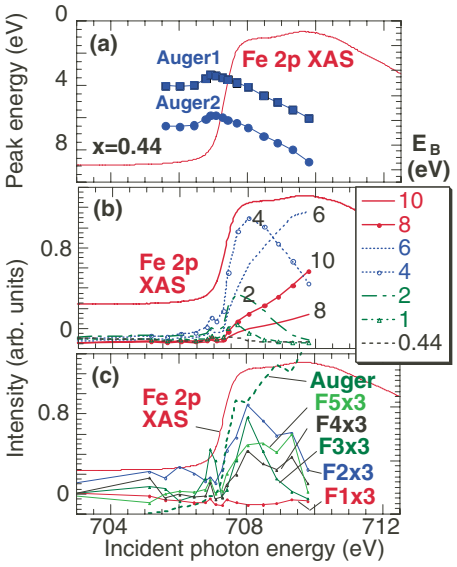

FIG. 6. (Color online) Results of analyses for $x=0.44$ as a function of the incident photon energies with the Fe $2p_{3/2}$ absorption spectra. (a) Peak energies of the Auger lines. (b) Change in the intensity of the constant initial states at given binding energies (E_B). The labeled numbers in the figure correspond to the binding energies. (c) Results of the curve fit in Fig. 4: change in the $F1-F5$ intensities with Auger intensity. Each F intensity is multiplied by a factor of 3. Two Auger line intensities are summed.

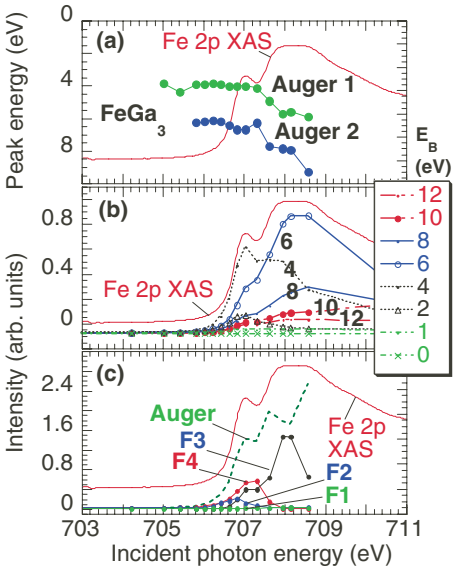

FIG. 7. (Color online) Results of analyses for $FeGa_3$ as a function of the incident photon energies with the Fe $2p_{3/2}$ absorption spectra. (a) Peak energies of the Auger lines. (b) Change in the intensity of the constant initial states at given binding energies (E_B). The labeled numbers in the figure correspond to the binding energies. (c) Results of the curve fit in Fig. 4: change in the $F1-F5$ intensities with Auger intensity. Two Auger line intensities are summed.

6 ($x=0.44$), and Fig. 7 ($FeGa_3$) with Fe $2p_{3/2}$ XAS spectra. Crossover points (COPs) between the Raman and Auger regions are estimated to be about 706 eV at $x=0$ and 707–707.8 eV at $x=0.44$, which are near the absorption edges of 706.58 eV at $x=0$ and 707.31 eV at $x=0.44$. Compared to the COP of a pure Fe metal (706.9 eV),[44] the COP at $x=0$ decreases, while that at $x=0.44$ remains nearly the same or slightly increases.

Weinelt *et al.*[45] observed the smooth transition from Raman to Auger at COP for Ni metal. Hüfner *et al.*[44] compared the COP with the $2p$ XAS peak for Cr, Fe, and Ni metals. The $2p$ XAS peak should usually coincide with the COP because of the many-body effects such as screening if there was no correlated hole. The COP of Ni was the same as the $2p$ XAS absorption peak because of the absence of correlated holes at the Ni Fermi edge. On the other hand, the COPs of Cr and Fe metals were below the $2p$ XAS absorption peaks due to the correlation of the holes. Similar observation was reported in the alloy of $Fe_{62}Ni_{20}Cr_{18}$.[46] They, however, showed that the alloying did not increase the delocalization at Fe $3d$ levels because the COP of Fe in this alloy agreed with that of Fe metal.

We note that their $2p_{3/2}$ XAS spectra showed a single peak. Our Fe $2p$ XAS spectra (total electron yields), however, show the structure at $2p_{3/2}$ peak as shown in Fig. 1(a). In our case the COPs are around the absorption edge. The COPs of FeSi and $FeSi_{1-x}Ge_x$ are almost the same as the Fe metal of about 706.9 eV,[44] indicating a similar correlation energy of holes and delocalized d states with Fe metal.

Figures 5(b) and 5(c) at $x=0$ show the change in the CIS at given binding energies and results of the curve fit for each component of $F1-F5$. Both the CIS and result of the curve fit show a similar behavior. High-resolution XAS spectra clearly demonstrated that two peaks, $p1$ and $p3$, are mainly associated with valence $3d$ and Auger electrons, respectively. The peak $p2$ seems to include both contributions.

Similar trend of the $x=0$ sample is also observed for the $x=0.44$ sample as shown in Fig. 6. We, however, observe two kinds of different behaviors for the $x=0.44$ sample. First the Raman region does not smoothly connect to the Auger region [Fig. 6(a)] and second Fano-type profile was observed [Figs. 6(b) and 6(c)]. In other words, we find that at COP both processes of Raman and Auger are mixed for the $x=0.44$ sample. This can be confirmed from the Fano-type profile.[45,47] The electron emissions from the valence band and the Auger process due to super-Coster-Kronig (LVV, V—valence) decay are written as $h\nu+3d^n \rightarrow 3d^{n-1}+e_k$ and $h\nu+np^63d^n \rightarrow np^53d^{n+1} \rightarrow np^63d^{n-1}+e_k$, where e_k is the emitted electrons. The interaction may occur between the discrete state (np^53d^{n+1}) and the continuum state ($np^63d^{n-1}+e_k$). They have the same initial and final states and thus the Fano profile could be observable if two processes are mixed. We do not observe the Fano-type profile for the $x=0$ sample. This fact indicates that the intermediate np^53d^{n+1} state has the broadening in energy at $x=0$ and is therefore delocalized compared to the state at $x=0.44$. The lattice constant increases with increasing the Ge doping.[20] The induced local lattice expansion around Ge ions causes the enhancement of the local DOS on their neighboring Fe sites that favors the appearance of magnetic moments. It also follows that Fe $3d$ state for the $x=0.44$ sample is relatively well localized compared to the $x=0$ sample. In both cases of $x=0$ and 0.44, however, the COPs are around the absorption edge and the

Raman region is restricted below the edge, suggesting the delocalization (covalence) of 3*d* states as a whole. It is noted that similar discussion about the degree of the delocalization or covalence can be seen in the resonant XES (including resonant inelastic x-ray scattering).[28,48]

On the other hand, $FeGa_3$ shows a different electronic structure. We do not observe the Fano-type profile for the $FeGa_3$ sample similarly to the $x=0$ sample. The contribution of the white peak of the absorption spectrum in $FeGa_3$ mainly consists of the Auger and partly includes the *F*3 component in Fig. 4(c) corresponding to Fe DOS.[32]

IV. CONCLUSION

We made the soft x-ray photoelectron spectroscopy for $FeSi_{1-x}Ge_x$ ($x=0$, 0.11, 0.19, 0.26, and 0.44) complementary for the XES and for $FeGa_3$ as a reference sample of a gap semiconductor. High-resolution XAS measurement at Fe $2p_{3/2}$ resolved the fine structure, corresponding to mainly the contributions from the valence of 3*d* and Auger electrons. We confirm the insulator to metal transition between $x=0.26$ and 0.44 in the valence-band spectra, where in the K_β XES the intensity of the up spin seemed to increase monotonously with Ge doping. The valence-band spectra indicate the narrowing of the DOS near the Fermi edge in agreement with the band calculations. Resonant PES is performed for the $x=0$ and 0.44 samples at Fe $2p_{3/2}$ absorption edge. We found *in CIS* that the Fano-type profile is observed only for $x=0.44$ sample around the point, indicating the crossover of the Raman and Auger features. On the other hand we do not observe the Fano-type profile for the $FeGa_3$ sample similarly to the $x=0$ sample. This indicates that at $x=0$ the intermediate state of $np^5 3d^{n+1}$ is not discrete and more delocalized compared to the state at $x=0.44$. The crossover point is near the absorption edge of Fe $2p$ for both of $x=0$ and 0.44, showing the delocalized 3*d* states.

ACKNOWLEDGMENTS

The experiments were performed at BL17SU (Proposals No. 2006B0044 and No. 2007A00081) of SPring-8 in the Japan Synchrotron Radiation Research Institute (JASRI). We thank Ignace Jarrige in JAEA for fruitful discussion.

[1] V. Jaccarino, G. K. Wertheim, J. H. Wernick, L. R. Walker, and S. Arajs, Phys. Rev. **160**, 476 (1967).
[2] U. Häussermann, M. Boström, P. Viklund, Ö. Rapp, and T. Björnängen, J. Solid State Chem. **165**, 94 (2002).
[3] Y. Nishino, M. Kato, S. Asano, K. Soda, M. Hayasaki, and U. Mizutani, Phys. Rev. Lett. **79**, 1909 (1997).
[4] C. Petrovic, J. W. Kim, S. L. Budko, A. I. Goldman, P. C. Canfield, W. Choe, and G. J. Miller, Phys. Rev. B **67**, 155205 (2003).
[5] *Semiconducting Silicides*, Springer Series in Materials Science Vol. 39, edited by V. E. Borisenko (Springer-Verlag, Berlin, 2000).
[6] K. Ishizaka, T. Kiss, T. Shimojima, T. Yokoya, T. Togashi, S. Watanabe, C. Q. Zhang, C. T. Chen, Y. Onose, Y. Tokura, and S. Shin, Phys. Rev. B **72**, 233202 (2005).
[7] L. F. Mattheiss and D. R. Hamann, Phys. Rev. B **47**, 13114 (1993).
[8] V. I. Anisimov, S. Y. Ezhov, I. S. Elfimov, I. V. Solovyev, and T. M. Rice, Phys. Rev. Lett. **76**, 1735 (1996).
[9] C. Fu and S. Doniach, Phys. Rev. B **51**, 17439 (1995).
[10] K. Urasaki and T. Saso, J. Phys. Soc. Jpn. **68**, 3477 (1999).
[11] T. Jarlborg, Physica B (Amsterdam) **293**, 224 (2001).
[12] M. Neef, K. Doll, and G. Zwicknagl, J. Phys.: Condens. Matter **18**, 7437 (2006).
[13] Y. Takahashi and T. Moriya, J. Phys. Soc. Jpn. **46**, 1451 (1979); Y. Takahashi, J. Phys.: Condens. Matter **9**, 2593 (1997); Y. Takahashi, *ibid.* **10**, L671 (1998); Y. Takahashi, T. Kanomata, R. Note, and T. Nakagawa, J. Phys. Soc. Jpn. **69**, 4018 (2000).
[14] G. Aeppli and Z. Fisk, Comments Condens. Matter Phys. **16**, 155 (1992).
[15] T. Jarlborg, Phys. Rev. B **51**, 11106 (1995).
[16] B. Lebech, J. Bharathi, and T. Freltoft, J. Phys.: Condens. Matter **1**, 6105 (1989).
[17] P. Pedrazzini, H. Wilhelm, D. Jaccard, T. Jarlborg, M. Schmidt, M. Hanfland, L. Akselrud, H. Q. Yuan, U. Schwarz, Yu. Grin, and F. Steglich, Phys. Rev. Lett. **98**, 047204 (2007).
[18] V. Guritanu, D. van der Marel, J. Teyssier, T. Jarlborg, H. Wilhelm, M. Schmidt, and F. Steglich, Phys. Rev. B **75**, 155114 (2007).
[19] P. Nordblad, L. Lundgren, and O. Beckman, Phys. Scr. **28**, 246 (1983).
[20] A. Bharathi, Awadhesh Mani, G. V. Narasimha Rao, C. S. Sundar, and Y. Hariharan, Physica B (Amsterdam) **240**, 1 (1997).
[21] E. Bauer, A. Galatanu, R. Hauser, Ch. Reichl, G. Wiesinger, G. Zaussinger, M. Galli, and F. Marabelli, J. Magn. Magn. Mater. **177-181**, 1401 (1998).
[22] Ch. Reichl, G. Wiesinger, G. Zaussinger, E. Bauer, M. Galli, and F. Marabelli, Physica B (Amsterdam) **259-261**, 866 (1999).
[23] A. Mani, A. Bharathi, and Y. Hariharan, Phys. Rev. B **63**, 115103 (2001); A. Mani, Solid State Commun. **132**, 551 (2004).
[24] V. I. Anisimov, R. Hlubina, M. A. Korotin, V. V. Mazurenko, T. M. Rice, A. O. Shorikov, and M. Sigrist, Phys. Rev. Lett. **89**, 257203 (2002).
[25] S. Yeo, S. Nakatsuji, A. D. Bianchi, P. Schlottmann, Z. Fisk, L. Balicas, P. A. Stampe, and R. J. Kennedy, Phys. Rev. Lett. **91**, 046401 (2003).
[26] T. Jarlborg, J. Magn. Magn. Mater. **283**, 238 (2004).
[27] H. Yamaoka, N. Tsujii, K. Yamamoto, H. Oohashi, A. M. Vlaicu, K. Kunitani, K. Uotani, D. Horiguchi, T. Tochio, Y. Ito, and S. Shin, Phys. Rev. B **76**, 075130 (2007).
[28] H. Yamaoka, N. Tsujii, H. Oohashi, D. Nomoto, I. Jarrige, K. Takahiro, K. Ozaki, K. Kawatsura, and Y. Takahashi, Phys. Rev. B **77**, 115201 (2008).
[29] C. S. Lue, W. J. Lai, and Y.-K. Kuo, J. Alloys Compd. **392**, 72 (2005).

[30] N. Tsujii, H. Yamaoka, H. Oohashi, I. Jarrige, D. Nomoto, K. Takahiro, K. Ozaki, and K. Kawatsura, Physica B (Amsterdam) **403**, 922 (2008).
[31] N. Tsujii, H. Yamaoka, M. Matsunami, R. Eguchi, Y. Ishida, Y. Senba, H. Ohashi, S. Shin, T. Furubayashi, H. Abe, and H. Kitazawa, J. Phys. Soc. Jpn. **77**, 024705 (2008).
[32] Y. Imai and A. Watanabe, Intermetallics **14**, 722 (2006).
[33] H. Ohashi, Y. Senba, H. Kishimoto, T. Miura, M. Takeuchi, K. Takeshita, S. Goto, S. Takahashi, H. Aoyagi, M. Sano, Y. Furukawa, T. Ohata, T. Matsushita, Y. Ishizawa, S. Taniguchi, Y. Asano T. Takeuchi, M. Oura, K. Shirasawa, T. Tanaka, Y. Harada, T. Tokushima, K. Horiba, H. Kitamura, T. Ishikawa, and S. Shin, in *Synchrotron Radiation Instrumentation: 9th Int. Conf. Synchrotron Radiation Instrumentation*, AIP Conf. Proc. No. 879 (AIP, Melville, NY, 2007), p. 523.
[34] K. Horiba, N. Kamakura, K. Yamamoto, K. Kobayashi, and S. Shin, J. Electron Spectrosc. Relat. Phenom. **144-147**, 1027 (2005).
[35] C. Fu, M. P. C. M. Krijn, and S. Doniach, Phys. Rev. B **49**, 2219 (1994).
[36] T. Åberg and B. Crasemann, in *Resonant Anomalous X-Ray Scattering Theory and Application*, edited by G. Materlik, C. J. Sparks, and K. Fischer (Elsevier, Amsterdam, 1994), p. 431.
[37] M. Ohno, J. Electron Spectrosc. Relat. Phenom. **148**, 41 (2005).
[38] M. Finazzi, N. B. Brookes, and F. M. F. de Groot, Phys. Rev. B **59**, 9933 (1999).
[39] M. Finazzi, G. Ghiringhelli, O. Tjernberg, P. Ohresser, and N. B. Brookes, Phys. Rev. B **61**, 4629 (2000).
[40] A. Kotani and Y. Toyozawa, J. Phys. Soc. Jpn. **37**, 912 (1974).
[41] S. Hüfner, *Photoelectron Spectroscopy* (Springer-Verlag, Berlin, 1994), p. 74.
[42] V. Ilakovac, M. Kralj, P. Pervan, M. C. Richter, A. Goldoni, R. Larciprete, L. Petaccia, and K. Hricovini, Phys. Rev. B **71**, 085413 (2005).
[43] T. Saitoh, A. Sekiyama, T. Mizokawa, A. Fujimori, K. Ito, H. Nakamura, and M. Shiga, Solid State Commun. **95**, 307 (1995).
[44] S. Hüfner, S.-H. Yang, B. S. Mun, C. S. Fadley, J. Schäfer, E. Rotenberg, and S. D. Kevan, Phys. Rev. B **61**, 12582 (2000).
[45] M. Weinelt, A. Nilsson, M. Magnuson, T. Wiell, N. Wassdahl, O. Karis, A. Föhlisch, N. Mårtensson, J. Stöhr, and M. Samant, Phys. Rev. Lett. **78**, 967 (1997).
[46] V. Formoso, G. Chirarello, R. G. Agostino, L. Papagno, E. Colavita, L. Floreano, R. Gotter, A. Morgante, A. Santaniello, and A. Verdini, Eur. Phys. J. B **43**, 463 (2005).
[47] S. Pagliara, L. Sangaletti, A. Goldoni, C. Kim, Z.-X. Shen, A. Revcolevschi, G. Dhalenne, and F. Parmigiani, Phys. Rev. B **65**, 205107 (2002).
[48] J.-P. Rueff, L. Journel, P.-E. Petit, and F. Farges, Phys. Rev. B **69**, 235107 (2004).